Chemical Identification of Single Ultrafine Particles Using Surface-Enhanced Infrared Absorption

Christian Huck,[1,*] Michael Tzschoppe,[1] Rostyslav Semenyshyn,[2] Frank Neubrech,[1] and Annemarie Pucci[1]

[1] *Kirchhoff Institute for Physics, University of Heidelberg, Im Neuenheimer Feld 227, 69120 Heidelberg, Germany*

[2] *4th Physics Institute and Research Center SCoPE, University of Stuttgart, Pfaffenwaldring 57, 70569 Stuttgart, Germany*

In the past decade, it has been demonstrated that surface-enhanced infrared absorption (SEIRA) is a powerful method to enhance vibrational signals of thin molecular layers. Much less attention has so far been given to the possibility of using SEIRA for the detection and characterization of nanometer-sized particles, such as ultrafine dust particles. Here, we report on SEIRA measurements demonstrating that even one single particle with a deeply subwavelength dimension of less than 100 nm can be detected and chemically characterized with standard infrared microspectroscopy. Our approach is based on plasmonic resonances of bowtie-shaped Au apertures that are designed to extraordinarily enhance the material-specific phononic excitations of a nanometer-sized silica particle. We show that the bowtie geometry is especially suited for single-particle spectroscopy, as it combines the advantage of an intense electromagnetic hot spot, the size of which can be adjusted to the particle dimension, with easy positioning of ultrafine dust particles inside that hot spot. In agreement with numerical calculations, we show that a detection limit in terms of a particle diameter of less than 20 nm can be achieved, which corresponds to a ratio of the diameter to the vacuum wavelength below 0.002. Our approach offers the possibility of analyzing infrared bands from tiniest particles and thus paves the way toward SEIRA-based devices that can sense ultrafine dust.

I. INTRODUCTION

Triggered by the technical progress that has allowed the accurate design of nanostructures, interest in the field of plasmonics and plasmonic coupling has grown strongly over recent decades. Due to the possibility of concentrating electromagnetic fields in deeply subwavelength volumes, a large number of possible applications have emerged. For example, the plasmonic near-field enhancement of nanostructures has been used to increase the sensitivity of photodetectors [1], to probe local chemical reactions [2], to enhance the efficiency of solar cells [3,4], and can even be helpful in cancer therapy [5]. The most promising applications in chemical sensing are based on surface-enhanced Raman spectroscopy (SERS) and surface-enhanced infrared (IR) spectroscopy (SEIRA) with resonant plasmonic nanostructures. In SEIRA measurements, molecular vibrational signals are enhanced by coupling the vibrational excitation to the plasmonic one via the strong electromagnetic field of the plasmonic excitation. The coupling can be interpreted in analogy to a

Fano-type interaction [6]. Great efforts have been made to bring the detection limit closer to the single-molecule level—as demonstrated, for example, by SERS [7,8] and enhanced fluorescence [9], respectively. Several research groups have already pushed the SEIRA detection limit toward the detection of only a few molecules. They have used highly sophisticated geometries in order to concentrate the resonant near field and so to enhance the coupling further [10]. Starting from linear nanoantennas [6,11], sensitivity was improved by using fan-shaped nanoantennas [12], nanoslits [13], and nanostructures above reflective substrates [14]. The most promising approach regarding single-molecule detection is given by coupled nanostructures, which are separated by a nanometer-sized gap [10,15,16]. Recently, Dong *et al.* [17] have made an important step toward single-molecule SEIRA detection by showing that as few as 500 molecules can be detected by using bowtie-shaped Au structures with a sub-3-nm gap into which the near field is confined.

Bowtie-shaped nanoantennas have not only been used to enhance IR vibrational signals but have also been the subject of various other studies, such as gap-dependent optical coupling [18], the huge near-field enhancement studied, for

_____

*christian.huck@kip.uni-heidelberg.de

example, by two-photon-excited photoluminescence [19], and near-field scanning optical microscopy [20]. Driven by the high near-field enhancement, further applications such as single-molecule fluorescence [9], few-molecule SERS [21], a boosted photocatalytic efficiency [22], and a three-dimensional gap plasmon that enables extreme confinement with a modal volume of about $4 \times 10 \times 10$ nm^3, corresponding to $1.3 \times 10^{-7} \lambda^3$ [23], have been demonstrated.

In addition to the particle-based bowtie antennas, bowtie apertures, working according to Babinet's principle, have also been investigated [24]. This inverse antenna design is well suited, for example, for the enhancement and confinement of magnetic fields [25,26]. Moreover, bowtie apertures have a great potential for SEIRA, as suggested by Cetin *et al.* [27]. Nevertheless, bowtie apertures have not been used for SEIRA experiments up to now.

Most of the SEIRA experiments presented so far aim to enhance vibrational signals of thin but laterally extended molecular layers, such as protein layers, for example [28,29]. However, the detection and characterization of solid nanoparticles, such as fine dust particles, is also an important but not-recognized field of application. A few years ago, single airborne dust particles with a size in the micrometer range [30,31] were investigated by IR spectroscopy and, recently, Vogt *et al.* have successfully demonstrated the chemical identification of individual silica particles with a diameter of approximately 240 nm in resonantly excited nanoslits by their enhanced-particle phonon-polariton signals [32,33]. However, the experimental step toward the detection of ultrafine dust particles with a diameter below 100 nm has still not been done, although this step might open up new areas of application in, for example, the fields of astronomy, environmental physics, and also medicine, where ultrafine dust plays an important role due to the large impact of the smallest dust particles on environmental safety and respiratory diseases as well as cardiovascular health [34–36]. It is known that ultrafine particles are the main constituent of airborne particulate matter and, due to their quantity and their ability to penetrate deep within the lung, they are a major concern for respiratory exposure and health. Exposure to crystalline silica particles in particular is known to be a health risk in many industrial environments [37,38]. Therefore, attention has been drawn to IR-spectroscopic investigation of silica ultrafine particles in recent publications [39,40].

In this contribution, we experimentally demonstrate that single ultrafine dust particles down to a diameter of 34 nm can be chemically characterized by SEIRA measurements utilizing tailored bowtie nanoapertures. On the basis of experimental IR spectra and near-field simulations for the plasmonic resonance, we provide design rules for the optimum bowtie geometry for the detection of ultrafine dust particles with diameters down to 15 nm. For the optimum design, it is important to increase the coupling between

the plasmon-polaritonic excitation of the metallic bowtie structure and the phonon-polaritonic excitation of the silica sphere. This means that both resonances have to overlap in energy and in volume. Optimum volume overlap is achieved when the sphere occupies the volume of the confined plasmonic near field. An easy method is applied for positioning nanoparticles with diameters of less than 100 nm in the hot spots of the bowtie apertures.

II. EXPERIMENTAL METHODS

A. Bowtie nanoaperture fabrication

Bowtie nanoapertures are fabricated on a CaF$_2$(100) crystal (coated with 2.5 nm of Cr and 50 nm of Au) by electron-beam lithography (EBL) and a subsequent argon-ion etching step. The details of the fabrication process can be found in Ref. [13]. In order to overcome limitations due to the proximity effect, we proceed as follows. Instead of an exposure of the whole nanobowtie, a pair of triangular-shaped patterns are exposed (see Fig. S1 in the Supplemental Material [41]). By varying the distance between the two triangles, bowtie nanoapertures with gap sizes down to 20 nm are successfully prepared. During the dry-etching process, we remove 15 nm of the underlying CaF$_2$ substrate additional to the Au/Cr layer for two reasons. First, this guarantees that the aperture is not short-circuited by gold residuals and, second, the silica spheres with a diameter of 85 nm used in this work are perfectly centered in the *z* direction. The etching depth is controlled by AFM measurements (see Fig. S2 in the Supplemental Material [41]).

B. Positioning of silica nanospheres

Silica particles are used as the model system for two reasons. First, the particles are available in nearly any size, with a very small size distribution. Second, the particles show one prominent absorption band, making data evaluation straightforward. Beside these advantages, our approach can be used to characterize any material that provides infrared vibrational bands. The procedure for silica-sphere positioning is depicted in Fig. 1. Silica nanoparticles with a diameter of $d = 85$ nm (monomodal size distribution with polydispersity index < 0.2) are obtained as a powder from micromod Partikeltechnologie GmbH and are dissolved in ultrapure water with a solid content of approximately 0.1 mg/ml. Smaller particles are obtained as an aqueous suspension and are diluted to a solid content of 0.025 mg/ml. A droplet with a volume of 100 μl of the aqueous suspension is pipetted onto the bowtie nanoaperture sample and the spheres are allowed to settle into the nanostructures by waiting for 60 s. Afterward, the sample is rotated at 3000 rpm for 60 s. This step removes the water and all the spheres that are not located inside a nanostructure, by centrifugal forces. Nanoparticles
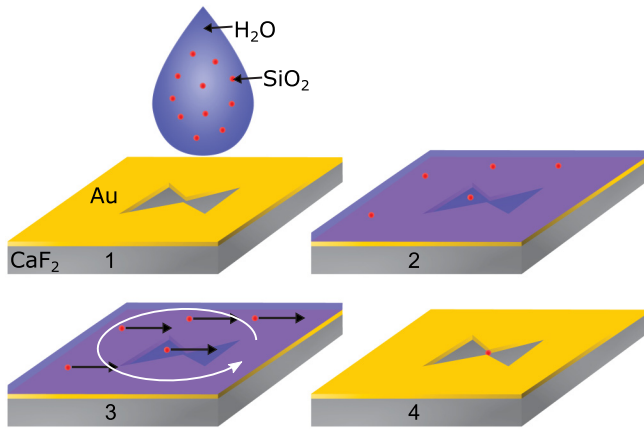
FIG. 1. The positioning of the silica spheres. The spheres are moved by centrifugal forces through the bowtie structure, where they get stuck in the center of the bowtie due to the tapering part.

located inside a nanostructure are accelerated to the outer end of the nanostructure. If a particle is located in the inner triangle of the bowtie structure, it is accelerated toward the tapering part of the bowtie. If the tapering part has a smaller dimension than the nanoparticle, it serves as a built-in trap, where the silica spheres are caught. Ideally, the dimension of the tapering part is only marginally smaller than the diameter of the sphere. In this case, the spheres are caught precisely in the center of the bowtie, where the highest near-field intensity is expected. The success rate of the approach is strongly dependent on the above-mentioned parameters, e.g., the sphere concentration and the settling time. The parameters are carefully chosen to get a single particle within the bowtie. The success rate of the approach is about 2–5%, which can be increased by further optimizing the parameters.

C. IR reflection spectroscopy

IR-spectroscopic measurements are carried out using a commercial Fourier-transform IR spectrometer (Bruker Tensor 27) coupled to an IR microscope (Bruker Hyperion 1000). Light emitted from a thermal light source is polarized with the electric-field vector parallel to the triangle base side and focused onto the sample using a ×36 reverse-Cassegrain objective. Reflected light is collected by the same objective and is detected by a liquid-nitrogen-cooled mercury-cadmium-telluride (MCT) detector. The whole beam path is purged with dried air in order to avoid atmospheric water and carbon dioxide absorption. Selected bowtie nanoapertures are roughly located using white-light microscopy followed by a precise alignment of the bowties into the center of the IR beam, the extent of which is specified by a circular aperture with a diameter of 12.5 μm. For details of the alignment procedure, see, e.g., Ref. [42]. Spectra are recorded with a resolution of 8 cm^{-1} and at least 100 000 scans (over about 12 hours). The relative

reflectance is calculated by normalizing the reflectance of the bowtie nanoaperture to the reflectance of the bare gold substrate.

Additional to the thermal light source, synchrotron radiation from the SOLEIL synchrotron is used, which allows us to reduce the number of scans and thus the measurement time by a factor of 25. More sophisticated light sources such as mid-IR lasers might allow us to further reduce the measurement time [43,44].

D. Numerical simulations

To confirm the experimental findings and to exactly determine the optimal antenna design, numerical studies are carried out using a commercial-grade simulator based on the finite-difference time-domain method (Lumerical's FDTD SOLUTIONS v.8.17.110) [45]. The CaF$_2$-substrate is modeled as a semi-infinite half space and is described as a dispersionless medium with a constant refractive index of $n = 1.41$. A 50-nm-thick gold layer is placed on top and described by a Drude model with a dielectric background of $\varepsilon_\infty = 7.0$, a plasma frequency of $\omega_p = 67900$ cm^{-1}, and a scattering rate of $\omega_\tau = 384$ cm^{-1} [46]. The geometry of the bowtie nanoaperture is defined by the base side b and the length L as well as the gap size in the center of the structure. To avoid nonphysical extremely high electric fields at sharp corners, the tips at the center of the bowtie are rounded (for further details on the simulation geometry, see also Fig. S3 and the text in the Supplemental Material [41]). Spherical silica spheres are placed at the center of the bowtie structure. The dielectric function of the silica spheres is taken from Ref. [32]. As the dielectric function depends on the manufacturing method of the silica spheres, minor differences are likely and are one reason for slight deviations between experiment and simulation. The phonon-polaritonic resonance of a very small sphere in vacuum is known as the Fröhlich resonance, the resonance frequency of which is given by the properties of the optical phonons of the material. At about 1100 cm^{-1}, the Si–O–Si stretching vibration is excited.

The total field scattered field approach is applied in order to calculate accurate scattering and absorption cross sections (for details, see Ref. [13]), which are then converted to a relative reflectance spectra by $R_{\text{rel}} = 1 - \sigma_{\text{ext}}/A_0$, where A_0 denotes the area of the measurement spot used in the respective experiment. A high-performance cluster (bwForCluster) is necessary to conduct the extensive numerical studies.

III. RESULTS AND DISCUSSION

Our device used for ultrafine-dust sensing is based on bowtie-shaped nanoapertures. The most obvious advantage of bowtie apertures is the extremely high electromagnetic-field intensity at the center of the structure. This advantage is illustrated in Fig. 2(a), which
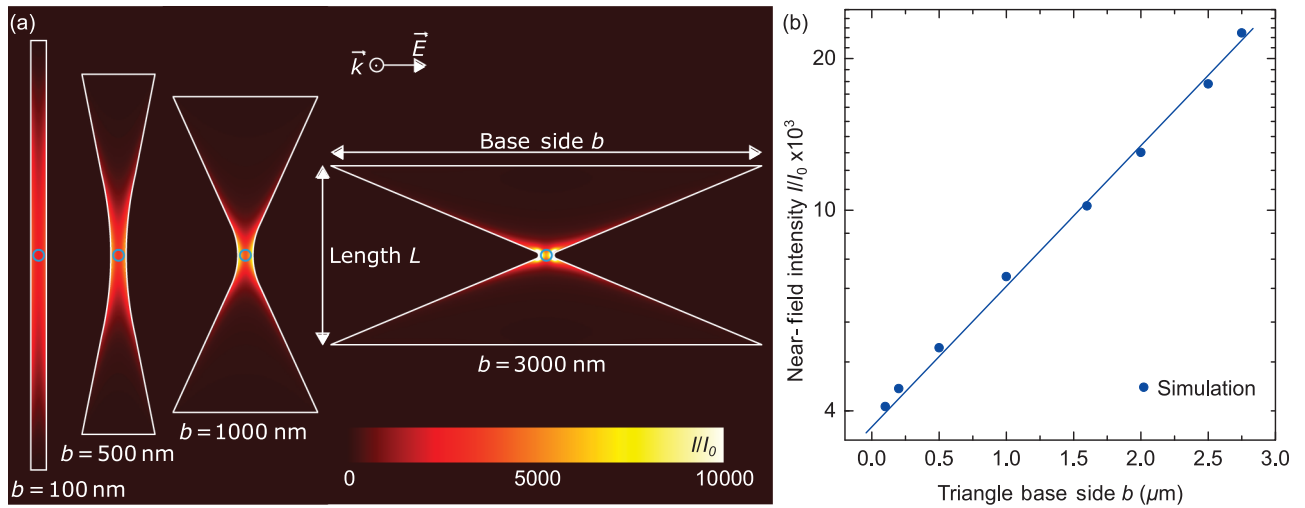
FIG. 2. The calculated near-field intensity of nanobowtie antennas for the electric-field direction ($\vec{E}$) as indicated. (a) The normalized near-field intensity distribution in a plane parallel to the substrate at the half height of the bowtie antenna. The base side of the bowtie is varied from 100 nm up to 3000 nm, whereas the length is adjusted to achieve a constant resonance frequency of $\omega_{res} = 1100$ cm^{-1}. The hot spot changes from an extended hot spot with low intensity to a highly localized hot spot with high intensity. For comparison, the size of an ultrafine dust particle is indicated by blue circles. (b) The near-field intensity read-out at the tapering part as a function of the bowtie base side b.

shows the simulated near-field intensity enhancement for various geometries, starting from a conventional linear nanoslit and ranging up to bowtie structures with increasing base side b. All of those geometries are designed to have the same resonance frequency matching to the resonance frequency of small silica particles (approximately 1100 cm^{-1}) [47], which are used as test particles throughout this paper. By increasing the base side b, the perimeter is increased, leading to a smaller resonance frequency [27]. In order to stay at a constant resonance frequency, this effect must be counterbalanced by a decreasing length L (for further information on resonance behavior of bowtie nanoapertures, see also Fig. S4). The linear nanoslit shows a very large near-field hot spot, which is almost spread over the entire slit length. This geometry that combines an extended hot spot with relatively high field intensities is beneficial, for example, for SEIRA measurements where thin molecular layers should be detected. The extended hot spot guarantees a good spatial overlap between the confined electromagnetic field and the molecular layer, resulting in high SEIRA signals, as shown, for example, in Ref. [13]. However, it is less suitable for single-particle detection, since the size of the hot spot is an order of magnitude larger than the area cross section of an ultrafine dust particle. To overcome this mismatch, one can change the geometry from a linear nanoslit to a bowtie-shaped structure. As shown in Fig. 2(a), increasing the length of the base side b leads to a more confined hot spot with a higher intensity. In order to quantitatively estimate how large the benefits of this geometry are compared to the linear nanoslit, it is useful to have a look at the near-field intensity generated by the different structures. To avoid unphysically

high values, sharp corners are rounded in the simulation geometry (see also Fig. S3). The near-field intensity is read out at the tapering part of the bowtie antennas, 2 nm away from the gold interface, and plotted against the triangle base side b in Fig. 2(b). The logarithmic plot shows an exponential increase of the near-field intensity with increasing base side b. By changing the geometry from a linear nanoslit geometry ($b = 100$ nm) to a pronounced bowtie geometry ($b = 3000$ nm), the near-field intensity is increased by a factor of more than 5. Simultaneously, the size of the hot spot becomes smaller, approaching the area cross section of an ultrafine dust particle.

To verify the suitability of this geometry experimentally, bowtie nanoapertures with different base sides ($b = 100$, 200, 500, 1000, and 2000 nm) are fabricated using a standard EBL approach with subsequent argon etching (for details, see Sect. II), as presented in Ref. [13]. The length of the bowties is adjusted between 1 and 3 μm to match the resonance frequency of the silica test particles, whereas the gap size at the tapering part is adjusted to match their diameter. In the next step, the silica spheres have to be positioned in the hot spot of the bowties. Typically, nano-objects can be positioned using a nanomanipulator with a very high accuracy of better than 50 nm, as applied by Vogt *et al.* [32]. However, if the particle dimensions fall below 100 nm, this approach reaches its limits and becomes time-consuming. Therefore, we use a strategy to position the ultrafine dust particles, which is suitable for all particle sizes and is tailored to the geometry of the bowtie apertures. As it turns out, the highly confined electromagnetic field is not the only advantage of bowtie apertures, regarding fine-dust sensing. Furthermore, the geometry can be

beneficial for the positioning of particles. By precisely adjusting the bowtie geometry to the particle size, the tapering part in the center of the bowtie can be used as a trap for particles (for details, see Sect. II). This works especially well if the gap size at the tapering part of the bowtie is slightly smaller than the diameter of the sphere. Furthermore, the capture cross section of a bowtie aperture is much bigger compared to that of a linear slit due to the much larger area cross section.

Figure 3 shows scanning-electron micrographs of silica nanospheres with a diameter of $d = 85$ nm positioned inside bowtie apertures by this technique. All of the spheres are nearly perfectly centered in the bowtie with the exception of the linear slit, where the missing tapering part hampers precise positioning. These results already clearly show one benefit of bowtie-shaped structures for ultrafine-dust sensing. Rarely, multiple particles may be located in one bowtie (in approximately 1% of the inspected bowties). This can be observed, for example,
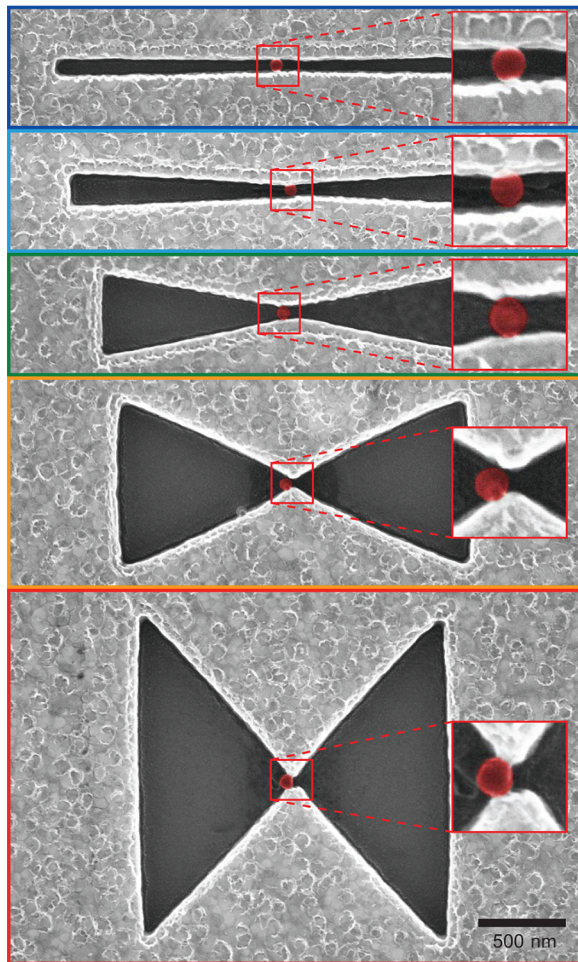
in the scanning-electron-microscopy (SEM) image of the $b = 1000$ nm bowtie. In Fig. S7 in the Supplemental Material [41], we show that such spheres do not contribute to the SEIRA signal and can therefore be neglected. Furthermore, in Fig. S6 in the Supplemental Material [41], we show that small sphere displacements due to gaps that are slightly too small do not hamper the enhancement of the spheres.

The IR optical properties of the different bowtie geometries shown in Fig. 3 are investigated by micro-IR spectroscopy (for details, see Sect. II) in reflectance geometry. According to Babinet's principle, the bowtie slit antennas feature a strong resonance when using light polarized perpendicular to the long axis [see Fig. 2(a)]. The spectra, which show a broadband plasmonic excitation, are shown in Fig. 4(a). By changing the geometry from the linear slit to the bowtie-shaped apertures, the plasmonic extinction increases slightly, which is a consequence of the increased geometric cross section of the bowties. The plasmonic excitation is modulated by the signature of

FIG. 3.   SEM images of bowtie antennas after sphere positioning. Bowties with a base side between 100 nm and 2 μm are fabricated and 85 nm silica spheres (colored red) are positioned at the center of the structures.
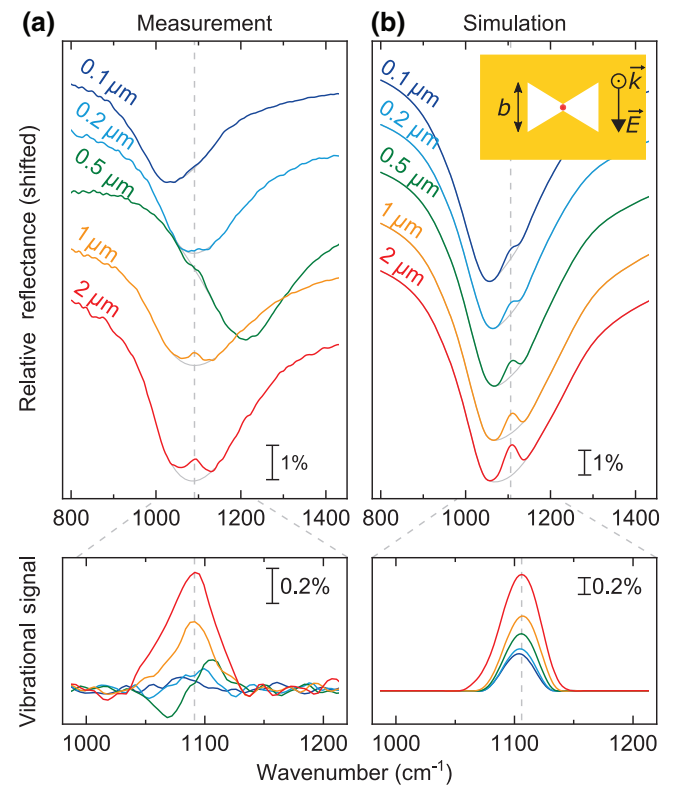

FIG. 4.   (a) The relative IR reflectance of the bowtie apertures shown in Fig. 3. A broad plasmonic resonance containing the Fano-type absorption peak of the silica sphere is observed. For the smallest ($b = 100$ nm), the signature of the silica sphere can barely be seen. However, the signal size increases if the base side of the bowtie structure is increased. The lower panel shows the baseline-corrected signal, where the increase in the signal can be seen clearly. The corresponding baseline is shown in gray in the upper panel. (b) FDTD simulations of the same geometry as shown in (a). The same trend as in the experimental data is found.

the sphere, which is visible as a Fano-type excitation at around 1100 cm^{-1}. This excitation corresponds to an enhanced localized surface phonon-polariton (for details, see Ref. [32,47]). In the Supplemental Material [41], we show that the optical properties of an ultrafine particle are determined by the dielectric function $\varepsilon(\omega)$ of the material, meaning that the spheres show the excitations that are characteristic for the material itself and therefore give the chemical information that IR spectroscopy can provide. The plasmonic resonance frequency perfectly matches this SiO_2 excitation, with the exception of the $b = 500$ nm bowtie, the manufactured length of which is too short, leading to a slightly higher plasmonic resonance frequency. Nevertheless, one can clearly see a trend for the signature of the silica spheres: For the bowtie geometry with $b = 100$ nm, corresponding to a nearly linear nanoslit, the signal of the silica sphere is nearly invisible, whereas a pronounced peak can be seen for the bowtie geometry with $b = 2000$ nm. This can be seen even more clearly in the baseline-corrected spectra, where the broadband plasmonic excitation is removed by dividing the measured spectra through a baseline representing the bare plasmonic resonance. To estimate a proper baseline, we use the asymmetric least-squares smoothing algorithm proposed by Eilers (see Ref. [48]), which has been established over recent years for the evaluation of SEIRA spectra [42,49,50]. The estimated baseline is shown within the figure as a light grey line; the baseline-corrected vibrational signals are shown in the lower panel of the figure. Obviously, the vibrational signal cannot be distinguished from noise for the bowtie with our smallest b, whereas a signal-to-noise ratio of 10 can easily be achieved for the bowtie with our largest b.

To confirm our measurement results and the important role of the coupling between the localized surface plasmon-polaritons (bowtie apertures) and the localized phonon-polaritons (silica spheres), we carry out finite-difference time-domain (FDTD) simulations (for details, see Sect. II). The results, presented in Fig. 4(b) next to the measurement data, confirm the trend that is observed in the experiment. The vibrational signal is extracted in the same way as in the experiment, by performing a baseline correction using the smoothing algorithm proposed by Eilers. Due to uncertainties of the baseline, the simulated vibrational signal can also be subject to minor errors. As observed in former studies [32], the simulated extinction of slit nanostructures tends to higher values than those observed in the experimental spectra. This can be explained by an imperfectly manufactured geometry in the experiment and differences of the real material optical properties of the structures as well as the beam alignment, which is one additional source of uncertainty in the experiment.

To quantitatively evaluate the enhanced vibrational signals of the silica spheres, the signal strengths (as peak-to-peak differences) are plotted in Fig. 5(a) against the triangle
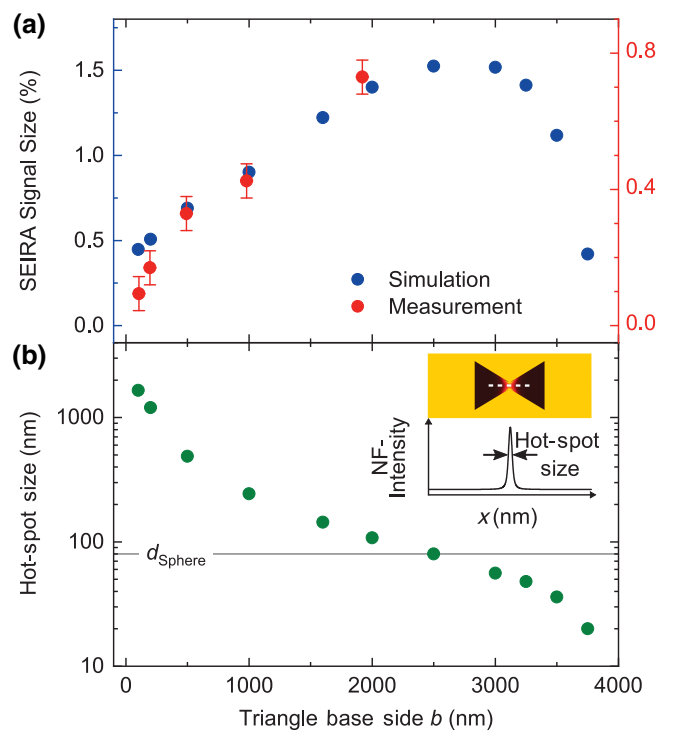

FIG. 5.   (a) The SEIRA signal-size read-out as the difference between the minimum and maximum of the baseline-corrected curve shown in Fig. 4. A strong increase of the SEIRA signal is observed for small values of b. For high values of b, the signal is decreasing again. The signal decrease can be explained by the size of the hot spot, which is shown in (b). An optimum SEIRA signal is found if the hot-spot size matches the sphere diameter.

base side b. By increasing b, the experimental and simulated data show an increase of the signal by factors of 7.8 and 3.5, respectively. The deviations may originate from imperfect positioning of the spheres in the linear nanoslit (see also Fig. 3). This might have decreased the signal for the $b = 100$ nm bowtie, which in turn leads to a higher signal increase when compared to the other geometries.

Interestingly, the simulated data show a decrease of the vibrational signal if one increases the base-side parameter b further. A maximally enhanced vibrational signal in our simulations is found for the bowtie geometry with $b = 2500$ nm. For higher values, the enhanced vibrational signal drops down rapidly, which can be explained by two factors. First, the hot spot becomes so small that the silica sphere no longer fits inside [Fig. 5(b)]. For this purpose, the hot-spot size is defined as the full width at half maximum of the near-field intensity [the line along the L axis; see the inset of Fig. 5(b)]. The maximum SEIRA signal is achieved if the hot-spot size matches the sphere diameter. Interestingly, the area cross section of the bowtie antenna follows the same trend as the SEIRA-signal (see Fig. S5 in the Supplemental Material [41]). The bowtie

with the highest area cross section features the highest SEIRA signal. Coming from small values of b, the area cross section increases with increasing b, until it reaches its maximum value at $b = 2500$ nm. A further increase of b leads to a decrease of the area cross section, which is explained by the decreasing length of the bowtie geometry (see Fig. S5). The decrease in the length is necessary to achieve the required resonance frequency, specified by the vibrational frequency of the silica particle. It is important to note that the optimum bowtie geometry is dependent on the size of the ultrafine dust particle as well as on the vibrational frequency of the mode of interest. In accordance with Fig. 5, the optimum geometry to detect much smaller particles should be given by a larger b compared to the value found here.

Spheres with different diameters are placed in the center of bowtie antennas to determine the limit of detection. For this purpose, we fabricate bowties with a base side of $b = 1000$ nm. The structure geometry stays the same as before, except for the size of the gap, which is adjusted to the diameter of the spheres. Adjusting the gap size guarantees an optimum capture cross section, enabling us to easily position the spheres in the hot spot of the bowties. SEM images of three different spheres with diameters of $d = 34$, 55, and 85 nm are shown in Fig. 6(a). The corresponding IR spectra are shown in Fig. 6(b). The vibrational signals of all three spheres can already be seen easily in the spectra, directly as measured, although the sphere signal is decreasing with decreasing sphere diameter. For a quantitative evaluation, the spectra are again baseline corrected, revealing a signal-to-noise ratio of better than 2 for the smallest sphere. If the sphere diameter is set in relation to the wavelength, it is found that in this measurement a particle is detected with a ratio of $d/\lambda \approx 0.0037$; therefore, this is a particle the cross section of which is nearly 5 orders of magnitude smaller than the wavelength squared.
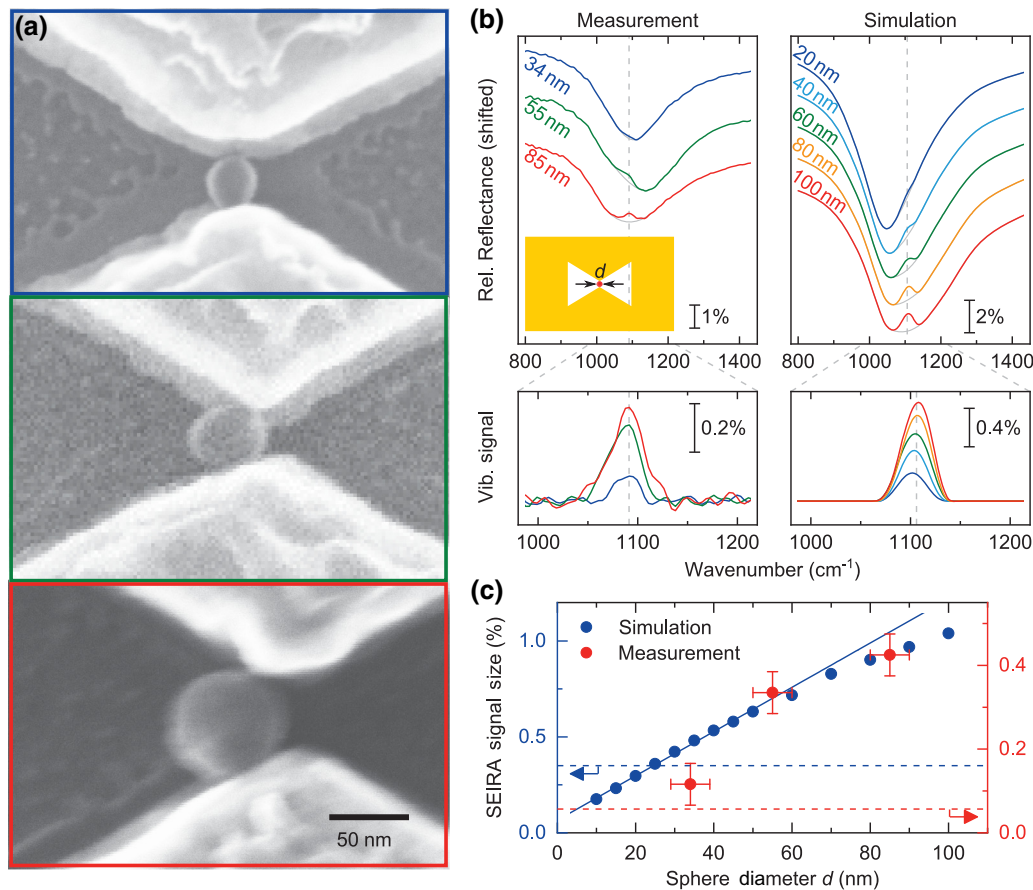

FIG. 6.   The detection limits. (a) SEM images of nanospheres positioned in the bowtie gap ($b = 1000$ nm, $L = 2100$ nm). The sphere diameter is changing from 34 nm through 55 nm to 85 nm. (b) The IR relative reflectance spectra and the baseline-corrected vibrational signal of the structures shown in (a). The signal of the smallest sphere is only slightly above the noise level, whereas the bigger spheres can easily be detected. The right-hand panel shows the corresponding FDTD simulations. (c) The SEIRA signal-size read-out from (b) plotted against the sphere diameter. The simulated signal is linearly increasing up to $d = 50$ nm. The red dashed line indicates the noise level of the experiment, whereas the blue dashed line indicates the detection limit of the simulated data, which we choose to be in accordance with the experimental data.

In order to confirm our experimental data on the dependency of the signal on the sphere diameter and to find a geometry-dependent detection limit, we carry out further FDTD simulations, assuming perfectly symmetric bowties with the sphere centered in the bowtie gap. The results are shown in Fig. 6(b). As in the experiment, a decreasing signal of the sphere is observed for a decreasing sphere diameter. Interestingly, the resonance frequency of the sphere decreases with a decreasing sphere diameter, corresponding to a shift toward the transversal optical phonon frequency [51]. This can be understood in the framework of the Mie theory, where an increasing sphere diameter leads to an increasing scattering contribution to the total extinction, shifting the Mie resonance frequency to higher values [52]. In turn, this allows us to estimate the sphere diameter via a precise measurement of the optical response of the silica spheres, in a nondestructive and label-free way.

By looking at the SEIRA signal size [Fig. 6(c)], one sees a linear increase for the SEIRA signal up to a sphere diameter of 50 nm. For larger diameters, a flattening of the curve can be observed, which can be explained by the height of the bowties, which limits the hot-spot volume. A comparison of the experimental and the simulated data shows that the signal of the smallest sphere used in the experiment is smaller than expected. This overly small signal is a result of the fact that the etching depth of the bowtie antennas is optimized for a sphere diameter of 85 nm, resulting in a geometry in which the small spheres are lying below the bowtie aperture (see Fig. S2). Therefore, for an optimized geometry, we expect a much bigger signal for the smallest sphere under investigation and we expect that even smaller spheres can be detected.

To further optimize the nanobowties for single-particle dust detection, we perform FDTD simulations with varying particle diameters and bowtie base sides [Fig. 7(a)]. As expected, a signal increase is observed for all sphere diameters, when going to larger values of b. Note that the particle size is much smaller than the size of the hot spot, which is the limiting factor in the above-mentioned configurations. Assuming a noise level [determined from experimental data; horizontal line in Fig. 7(a)], we estimate a detection limit for each bowtie configuration [Fig. 7(b)]. Obviously, the detection limit can be improved by increasing the base side of the bowtie geometry. Whereas the linear nanoslit can only be used to detect ultrafine dust particles with a size bigger than 67 nm ($d/\lambda \approx 0.0074$), a bowtie with a base side of 2500 nm can be used to characterize particles with a diameter down to 15 nm, corresponding to $d/\lambda \approx 0.0017$.

This detection limit enables interesting applications, such as in the fields of cosmic dust and air pollution, and biological applications, for example, for the detection and chemical characterization of a single virus, which typically has a size of 20–100 nm.
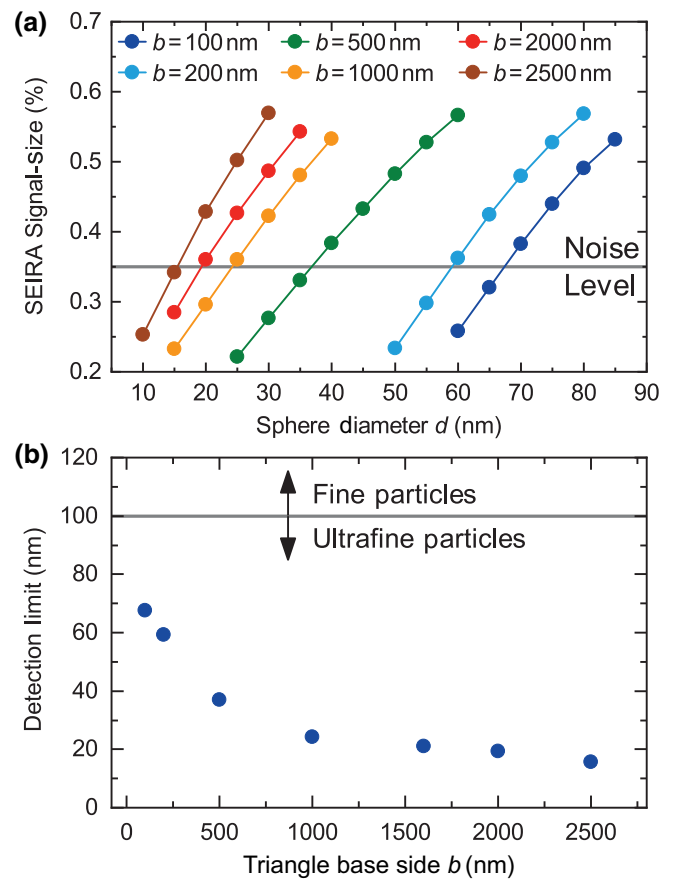

FIG. 7. The detection limit for silica particles. (a) The simulated SEIRA signal size of silica particles with an increasing diameter placed in the center of bowtie nanoapertures with different base sides b. The crossing point with the noise-level horizontal is defined as the detection limit and is plotted in (b) as a function of the triangle base side b. By increasing the base side, the detection limit can be improved down to a sphere diameter of less than 20 nm for the most powerful bowties ($b = 2500$ nm).

In order to demonstrate the chemical specificity for a more complex material than SiO_2, the upper panel of Fig. 8 shows the calculated extinction cross section of an ultrafine particle with $d = 50$ nm consisting of the organic material 4,4′-bis(N-carbazolyl)-1,1′-biphenyl (CBP) (for details of the calculation, see the Supplemental Material [41]). The middle panel of Fig. 8 shows the simulated relative-reflectance spectra of such a sphere placed into different bowtie antennas with $b = 2500$ nm together with the baseline-corrected vibrational signal shown in the lower panel. Although CBP features only weak IR-vibrational bands (marked by dashed vertical lines), the SEIRA spectrum clearly shows the characteristic bands, allowing us to unambiguously identify the material. A comparison of the calculated extinction cross sections of fine dust particles for a selection of other materials, including a polymer, two phononic materials, and the organic small molecule CBP, can be found in Fig. S8 of the Supplemental Material [41].
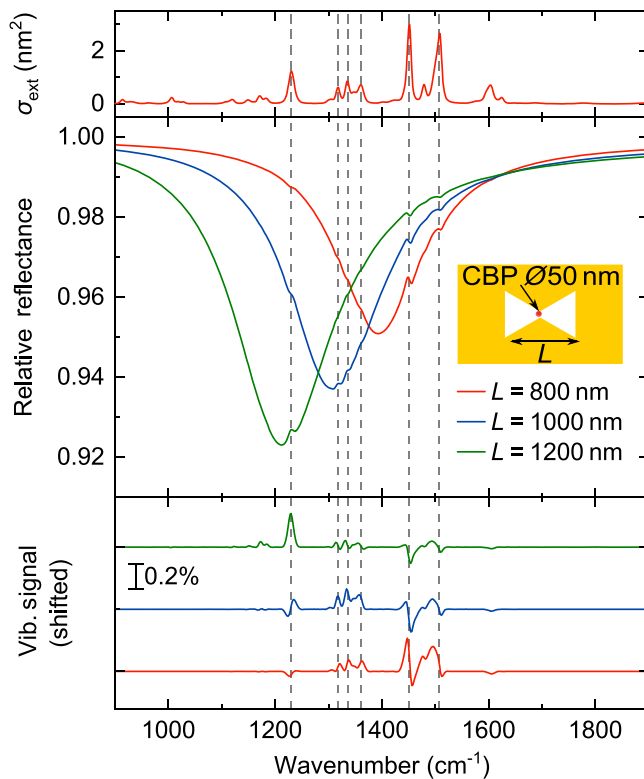
FIG. 8. The calculated extinction cross section of a fine dust particle with a diameter of 50 nm consisting of the organic material CBP (upper panel). The middle panel shows FDTD simulations of such a CBP sphere in bowtie antennas with $b = 2500$ nm and different lengths. The lower panel shows the baseline-corrected vibrational signal. The strongest vibrational bands of CBP are marked with dashed lines and can be used to identify and characterize the molecular species.

IV. SUMMARY AND CONCLUSION

In this work, we demonstrate a SEIRA platform based on bowtie nanoapertures for the detection and chemical characterization of ultrafine dust particles with diameters well below 100 nm. We show that bowtie nanoapertures offer clear advantages with regard to the detection of such small particles by plasmonic enhancement, because such nanoapertures provide a high electromagnetic field strength at the center of the nanostructure. By changing the bowtie geometry, the size of this hot spot can be influenced and thus can be adjusted to the size of the particle under investigation, which guarantees an optimum SEIRA enhancement. Furthermore, we reveal that the bowtie geometry features the possibility of easily capturing particles in the hot spot without the need for sophisticated positioning methods. By adjusting the gap size of the bowtie, the tapering part in the center acts as a trap to catch the particles. Through the use of this method, we position particles down to a diameter of 34 nm, which we thereupon characterize by far-field IR microspectroscopy.

With $d/\lambda < 0.0037$, this particle is the smallest one that has ever been characterized by far-field IR spectroscopy on a single-particle level. Through the use of FDTD calculations, we demonstrate that the detection limit can be further improved down to a particle diameter of 15 nm ($d/\lambda < 0.0017$) by optimizing the geometry. These results prove that the SEIRA-based characterization of ultrafine dust particles on a single-particle level is possible.

[1] L. Tang, S. E. Kocabas, S. Latif, A. K. Okyay, D.-S. Ly-Gagnon, K. C. Saraswat, and D. A. B. Miller, Nanometre-scale germanium photodetector enhanced by a near-infrared dipole antenna, Nat. Photonics **2,** 226 (2008).

[2] A. Tittl, X. Yin, H. Giessen, X.-D. Tian, Z.-Q. Tian, C. Kremers, D. N. Chigrin, and N. Liu, Plasmonic smart dust for probing local chemical reactions, Nano Lett. **13,** 1816 (2013).

[3] K. R. Catchpole and A. Polman, Plasmonic solar cells, Opt. Express **16,** 21793 (2008).

[4] Y. H. Jang, Y. J. Jang, S. Kim, L. N. Quan, K. Chung, and D. H. Kim, Plasmonic solar cells: From rational design to mechanism overview, Chem. Rev. **116,** 14982 (2016).

[5] A. M. Gobin, M. H. Lee, N. J. Halas, W. D. James, R. A. Drezek, and J. L. West, Near-infrared resonant nanoshells for combined optical imaging and photothermal cancer therapy, Nano Lett. **7,** 1929 (2007).

[6] F. Neubrech, A. Pucci, T. W. Cornelius, S. Karim, A. García-Etxarri, and J. Aizpurua, Resonant Plasmonic and Vibrational Coupling in a Tailored Nanoantenna for Infrared Detection, Phys. Rev. Lett. **101,** 157403 (2008).

[7] K. Kneipp, Y. Wang, H. Kneipp, L. T. Perelman, I. Itzkan, R. R. Dasari, and M. S. Feld, Single Molecule Detection Using Surface-Enhanced Raman Scattering (SERS), Phys. Rev. Lett. **78,** 1667 (1997).

[8] S. Nie, Probing single molecules and single nanoparticles by surface-enhanced Raman scattering, Science **275,** 1102 (1997).

[9] A. Kinkhabwala, Z. Yu, S. Fan, Y. Avlasevich, K. Müllen, and W. E. Moerner, Large single-molecule fluorescence enhancements produced by a bowtie nanoantenna, Nat. Photonics **3,** 654 (2009).

[10] F. Neubrech, C. Huck, K. Weber, A. Pucci, and H. Giessen, Surface-enhanced infrared spectroscopy using resonant nanoantennas, Chem. Rev. **117,** 5110 (2017).

[11] R. Adato, A. A. Yanik, J. J. Amsden, D. L Kaplan, F. G. Omenetto, M. K. Hong, S. Erramilli, and H. Altug, Ultrasensitive vibrational spectroscopy of protein monolayers with plasmonic nanoantenna arrays, PNAS **106,** 19227 (2009).

[12] L. V. Brown, X. Yang, K. Zhao, B. Y. Zheng, P. Nordlander, and N. J. Halas, Fan-shaped gold nanoantennas above reflective substrates for surface-enhanced infrared absorption (SEIRA), Nano Lett. **15,** 1272 (2015).

[13] C. Huck, J. Vogt, M. Sendner, D. Hengstler, F. Neubrech, and A. Pucci, Plasmonic enhancement of infrared vibrational signals: Nanoslits versus nanorods, ACS Photonics **2,** 1489 (2015).

[14] C. Huck, A. Toma, F. Neubrech, M. Chirumamilla, J. Vogt, F. De Angelis, and A. Pucci, Gold nanoantennas on a pedestal for plasmonic enhancement in the infrared, ACS Photonics **2,** 497 (2015).

[15] X. Chen, C. Ciracì, D. R. Smith, and S.-H. Oh, Nanogap-enhanced infrared spectroscopy with template-stripped wafer-scale arrays of buried plasmonic cavities, Nano Lett. **15,** 107 (2015).

[16] Y. Li, M. L. Simeral, and D. Natelson, Surface-enhanced infrared absorption of self-aligned nanogap structures, J. Phys. Chem. C **120,** 22558 (2016).

[17] L. Dong, X. Yang, C. Zhang, B. Cerjan, L. Zhou, M. L. Tseng, Y. Zhang, A. Alabastri, P. Nordlander, and N. J. Halas, Nanogapped Au antennas for ultrasensitive surface-enhanced infrared absorption spectroscopy, Nano Lett. **17,** 5768 (2017).

[18] D. P. Fromm, A. Sundaramurthy, P. J. Schuck, G. Kino, and W. E. Moerner, Gap-dependent optical coupling of single "bowtie" nanoantennas resonant in the visible, Nano Lett. **4,** 957 (2004).

[19] P. J. Schuck, D. P. Fromm, A. Sundaramurthy, G. S. Kino, and W. E. Moerner, Improving the mismatch between light and nanoscale objects with gold bowtie nanoantennas, Phys. Rev. Lett. **94,** 017402 (2005).

[20] E. X. Jin and X. Xu, Enhanced optical near field from a bowtie aperture, Appl. Phys. Lett. **88,** 153110 (2006).

[21] N. A. Hatab, C. H. Hsueh, A. L. Gaddis, S. T. Retterer, J. H. Li, G. Eres, Z. Zhang, and B. Gu, Free-standing optical gold bowtie nanoantenna with variable gap size for enhanced Raman spectroscopy, Nano Lett. **10,** 4952 (2010).

[22] C.-H. Lee, S.-C. Liao, T.-R. Lin, S.-H. Wang, D.-Y. Lai, P.-K. Chiu, J.-W. Lee, and W.-F. Wu, Boosted photocatalytic efficiency through plasmonic field confinement with bowtie and diabolo nanostructures under LED irradiation, Opt. Express **24,** 17541 (2016).

[23] M.-K. Kim, H. Sim, S. J. Yoon, S.-H. Gong, C. W. Ahn, Y.-H. Cho, and Y.-H. Lee, Squeezing photons into a point-like space, Nano Lett. **15,** 4102 (2015).

[24] H. Guo, T. P. Meyrath, T. Zentgraf, N. Liu, L. Fu, H. Schweizer, and H. Giessen, Optical resonances of bowtie slot antennas and their geometry and material dependence, Opt. Express **16,** 7756 (2008).

[25] N. Zhou, E. C. Kinzel, and X. Xu, Complementary bowtie aperture for localizing and enhancing optical magnetic field, Opt. Lett. **36,** 2764 (2011).

[26] T. Grosjean, M. Mivelle, F. I. Baida, G. W. Burr, and U. C. Fischer, Diabolo nanoantenna for enhancing and confining the magnetic optical field, Nano Lett. **11,** 1009 (2011).

[27] A. E. Cetin, S. Aksu, M. Turkmen, D. Etezadi, and H. Altug, Theoretical and experimental analysis of subwavelength bowtie-shaped antennas, J. Electromagn. Waves Appl. **29,** 1686 (2015).

[28] D. Rodrigo, O. Limaj, D. Janner, D. Etezadi, F. J. Garcia de Abajo, V. Pruneri, and H. Altug, Mid-infrared plasmonic biosensing with graphene, Science **349,** 165 (2015).

[29] D. Etezadi, J. B. Warner, IV, F. S. Ruggeri, G. Dietler, H. A. Lashuel, and H. Altug, Nanoplasmonic mid-infrared biosensor for *in vitro* protein secondary structure detection, Light: Sci. Appl. **6,** e17029 (2017).

[30] M. A. Malone, M. McCormack, and J. V. Coe, Single airborne dust particles using plasmonic metal films with hole arrays, J. Phys. Chem. Lett. **3,** 720 (2012).

[31] Joseph Heer, Lloyd Corwin, Katherine Cilwa, Marvin A. Malone, and James V. Coe, Infrared sensitivity of plasmonic metal films with hole arrays to microspheres in and out of the holes, J. Phys. Chem. C **114,** 520 (2010).

[32] J. Vogt, S. Zimmermann, C. Huck, M. Tzschoppe, F. Neubrech, S. Fatikow, and A. Pucci, Chemical identification of individual fine dust particles with resonant plasmonic enhancement of nanoslits in the infrared, ACS Photonics **4,** 560 (2017).

[33] H. Fröhlich, *Theory of Dielectrics* (Clarendon Press, Oxford, 1950).

[34] C. A. Pope and D. W. Dockery, Health effects of fine particulate air pollution: Lines that connect, J. Air. Waste. Manag. Assoc. **56,** 709 (2006).

[35] A. J. Cohen, H. Ross Anderson, B. Ostro, K. D. Pandey, M. Krzyzanowski, N. Künzli, K. Gutschmidt, A. Pope, I. Romieu, J. M. Samet, and K. Smith, The global burden of disease due to outdoor air pollution, J. Toxicol. Environ. Health Part A **68,** 1301 (2005).

[36] F. Dominici, R. D. Peng, M. L. Bell, L. Pham, A. McDermott, S. L. Zeger, and J. M. Samet, Fine particulate air pollution and hospital admission for cardiovascular and respiratory diseases, JAMA **295,** 1127 (2006).

[37] NIOSH, *NIOSH Hazard Review Health Effects of Occupational Exposure to Respirable Crystalline Silica* ((DHHS (NIOSH) Publication No. 2002129, Cincinnati, 2002).

[38] OSHA, *Occupational Exposure to Respirable Crystalline silica. Final Rule*, Federal Register 81, 16286 (Washington, 2016).

[39] S. Wei, P. Kulkarni, K. Ashley, and L. Zheng, Measurement of crystalline silica aerosol using quantum cascade laser–based infrared spectroscopy, Sci. Rep. **7,** 13860 (2017).

[40] A. L. Miller, N. C. Murphy, S. J. Bayman, Z. P. Briggs, A. D. Kilpatrick, C. A. Quinn, M. R. Wadas, E. G. Cauda, and P. R. Griffiths, Evaluation of diffuse reflection infrared spectrometry for end-of-shift measurement of α-quartz in coal dust samples, J. Occup. Environ. Hyg. **12,** 421 (2015).

[41] See the Supplemental Material at http://link.aps.org/supplemental/10.1103/PhysRevApplied.11.014036 for the scheme of the exposure procedure, the AFM measurements, the simulation geometry, the resonance behavior of bowtie

apertures, the geometrical details, the influence of sphere displacements, and the chemical identification of different materials.

[42] C. Huck, F. Neubrech, J. Vogt, A. Toma, D. Gerbert, J. Katzmann, T. Härtling, and A. Pucci, Surface-enhanced infrared spectroscopy using nanometer-sized gaps, ACS Nano **8**, 4908 (2014).

[43] A. Hasenkampf, N. Kröger, A. Schönhals, W. Petrich, and A. Pucci, Surface-enhanced mid-infrared spectroscopy using a quantum cascade laser, Opt. Express **23**, 5670 (2015).

[44] T. Steinle, F. Neubrech, A. Steinmann, X. Yin, and H. Giessen, Mid-infrared Fourier-transform spectroscopy with a high-brilliance tunable laser source: Investigating sample areas down to 5 μm diameter, Opt. Express **23**, 11105 (2015).

[45] Lumerical Solutions, Inc., http://www.lumerical.com/.

[46] J. Trollmann and A. Pucci, Infrared dielectric function of gold films in relation to their morphology, J. Phys. Chem. C **118**, 15011 (2014).

[47] A. Tamanai, J. Vogt, C. Huck, U. Mick, S. Zimmermann, R. Tazaki, H. Mutschke, and A. Pucci, Experimental verification of agglomeration effects in infrared spectra on micron-sized particles, Astron. Astrophys. **619**, A110 (2018).

[48] P. H. C. Eilers, A perfect smoother, Anal. Chem. **75**, 3631 (2003).

[49] J. Vogt, C. Huck, F. Neubrech, A. Toma, D. Gerbert, and A. Pucci, Impact of the plasmonic near- and far-field resonance-energy shift on the enhancement of infrared vibrational signals, Phys. Chem. Chem. Phys. **17**, 21169 (2015).

[50] B. Cerjan, X. Yang, P. Nordlander, and N. J. Halas, Asymmetric aluminum antennas for self-calibrating surface-enhanced infrared absorption spectroscopy, ACS Photonics **3**, 354 (2016).

[51] J. D. Caldwell, O. J. Glembocki, Y. Francescato, N. Sharac, V. Giannini, F. J. Bezares, J. P. Long, J. C. Owrutsky, I. Vurgaftman, J. G. Tischler, V. D. Wheeler, N. D. Bassim, L. M. Shirey, R. Kasica, and S. A Maier, Low-loss, extreme sub-diffraction photon confinement via silicon carbide localized surface phonon polariton resonators, Nano Lett. **13**, 3690 (2013).

[52] C. F. Bohren and D. R. Huffman, *Absorption and Scattering of Light by Small Particles* (Wiley-VCH, Weinheim, Germany, 2009).